




# Biothiol-mediated synthesis of Pt nanoparticles on graphene nanoplates and their application in methanol electrooxidation

Shengdong Dai<sup>1</sup> , Jinli Zhang<sup>1</sup>, Yan Fu<sup>1,\*</sup>, and Wei Li<sup>1,\*</sup> 

<sup>1</sup> School of Chemical Engineering and Technology, Tianjin University, Tianjin 300350, People's Republic of China

Received: 21 June 2017

Accepted: 22 August 2017

Published online:

1 September 2017

© Springer Science+Business Media, LLC 2017

## ABSTRACT

We synthesized highly dispersive Pt nanoparticles on graphene nanoplates (GNPs) under the orientation of different biothiols templates. Through the characterizations of FT-IR, ITC, HRTEM, EELS, XPS, cyclic voltammetry and chronoamperometry, it is demonstrated that the catalytic performance of GNPs-supported Pt NPs is greatly associated with thiol-containing groups, particle sizes as well as morphologies. There is a synergetic effect between biothiols and GNPs to modulate the dispersity and the distribution of Pt NPs. The biothiol-templated non-spherical Pt NPs on GNPs show higher activity and better stability in methanol oxidation reaction, comparing with those spherical Pt NPs formed in the solution and commercial Pt/C. Particularly for adopting cysteine as the biotemplate, Pt NPs show the highest catalytic activities as well as the enhanced antipoisoning property, with the mean width of 3 nm and the length ranging in 3–13 nm. These results pave a new way to manufacture hybrid nanocatalysts on the basis of facile modulation by biothiols.

## Introduction

Controllable synthesis of highly dispersive Pt-based nanocatalysts on two-dimensional carbon supports has gained considerable attention in the past decade, since supported Pt NPs are beneficial to enhancing catalytic efficiencies and stabilities during practical long-term operation, especially in electrooxidation reaction [1–4]. However, carbon supports, such as reduced graphene, graphene nanoplates, carbon nanotubes, lack sufficient functional groups for anchoring the precursors of metal ions, which leads to large NPs with low catalytic

activity [5]. To address this issue, growing interests lie in the chemical modification of inactive surfaces of carbon supports by ionic liquids [6, 7], conducting polymer [8], cyclodextrin [9, 10], pyrene-containing derivatives [11], DNA [12, 13], etc. These organic ligands act as capping agents to prevent Pt NPs from aggregation as well as to modulate their dispersion and distribution. For example, Li and coworkers employed polyaniline to modify multi-walled carbon nanotube as the template to synthesize Pt nanoparticles with the size about 3 nm, which showed higher electrochemical activity and lower CO poisoning susceptibility toward

Address correspondence to E-mail: fuyan@tju.edu.cn; liwei@tju.edu.cn

methanol oxidation reaction [14]. Yang and coworkers also used poly[2,2'-(2,6-pyridine)-5,5'-bibenzimidazole] (PyPBI)-functionalized multi-walled carbon nanotube to synthesize MWCNT/PyPBI/Pt. The carbon paper-free membrane electrode assembly (MEA) had comparable mass power density to that of the MEA with carbon paper [8]. Moreover, dispersive nanosized Pt NPs (1.9 nm) were synthesized on graphite nanoplatelets upon addition of an imidazolium-based ionic liquid, of which the electrocatalytic activity was 2.75 times higher than Pt/C toward the methanol oxidation reaction [6]. Concerning the unprecedented catalytic performance of Pt nanomaterials determined by surface states and morphology, it is desirable to develop new methods to tune the physicochemical properties of supported Pt NPs on the basis of molecular recognition abilities of functional groups.

Thiol-containing ligands, including glutathione (GSH), N-acetyl-L-cysteine, L-penicillamine, tiopronin, mercaptoammonium, L-cysteine as water-soluble ligands, and hexanethiol, dodecanthiol, 2-phenylethylthiol, methylbenzenethiol, phenylethanethiolate as organic-soluble ligands, have been recognized as promising capping agents for precisely controlling monodisperse metal nanoclusters/nanoparticles, which display both excellent stabilities and ultrasmall sizes [15–21]. For example, GSH-protected Pt NPs (2.3–3.6 nm) were synthesized in the aqueous solution, which showed the excellent peroxidase-like activity and the radical scavenging capability [22]. Recently, atomically precise Au nanocluster was successfully fabricated under the protection of  $-\text{SCH}_2\text{CH}_2\text{Ph}$  thiolates in toluene. Among these NPs,  $\text{Au}_{144}$  with the size of 1.7 nm exhibited the highest catalytic activities in both carbon monoxide oxidation and electrocatalytic oxidation of ethanol [23]. Therefore, we are motivated to employ thiol-containing ligands to modulate the physicochemical properties of carbon-supported Pt nanomaterials.

In this paper, we propose a simple and effective strategy on the controllable synthesis of highly dispersive Pt NPs on GNPs by using biothiols, including glutathione (GSH) and cysteine (Cys). Two different methods were comparatively studied to synthesize GNPs-supported Pt NPs, namely “adsorption–reduction” and “reduction–adsorption,” respectively. Through the characterizations of FT-IR, ITC, HRTEM, EELS, XPS, cyclic voltammetry and chronoamperometry, it is demonstrated that the catalytic performance of GNPs-supported Pt NPs is greatly associated with surface

functional groups, particle sizes as well as morphologies. The Cys/GNPs-guided Pt NPs with the average width of 3 nm and the length ranging in 3–13 nm display the highest catalytic activities in methanol electrooxidation. These results pave a promising way to manufacture 2D hybrid catalysts with facile modulation of physicochemical properties through biothiols.

## Experimental section

### Materials

Graphene nanoplates (GNPs, >99.5 wt% carbon content, width 0.5–20  $\mu\text{m}$ , thickness 1–5 nm, surface area 110  $\text{m}^2 \text{g}^{-1}$ , conductivity 80–100  $\text{S cm}^{-1}$ , zeta potential  $-19.6 \text{ mV}$ , ACS Material, USA) were sonicated for 2 h to decrease their sizes and aspect ratios (width to thickness).  $\text{K}_2\text{PtCl}_4$  (99.9%) was purchased from Alfa Aesar. L-cysteine (Cys) (99%) and reduced glutathione (GSH) were purchased from J&K Scientific LTD. The commercial catalyst (Pt/C-JM, 20 wt%) was purchased from Johnson Matthey. Ethylene glycol (EG), methanol ( $\text{CH}_3\text{OH}$ ) and other chemical reagents were purchased from Jiangtian Chemical Technology Co. Ltd (Tianjin, China). High-purity nitrogen ( $\geq 99.99\%$ ) was supplied by Tianjin Dongxiang Co. Ltd. All the chemical reagents were used without further purification. The water used in all experiments was distilled for three times.

### Synthesis of Pt-GSH/GNPs

#### Method I: adsorption–reduction

GSH was firstly incubated with 300  $\mu\text{M}$   $\text{K}_2\text{PtCl}_4$  at different molar ratios of  $[\text{GSH}]/[\text{K}_2\text{PtCl}_4]$  in 10 mM  $\text{NaH}_2\text{PO}_4\text{--H}_3\text{PO}_4$  buffer (pH 4.0) for 3 h at 25  $^\circ\text{C}$ . Then an equal volume of EG containing 15.7 mg sonicated GNPs was added to the above mixture. After vibration for 3 h at 25  $^\circ\text{C}$ , the resulting mixture was heated to 125  $^\circ\text{C}$  and reacted for 4 h under reflux. Finally, the resultant was filtered and the obtained solid was rinsed several times by  $\text{NaH}_2\text{PO}_4\text{--H}_3\text{PO}_4$  buffer (pH 4.0) and then dried at 60  $^\circ\text{C}$  under vacuum for 12 h.

#### Method II: reduction–adsorption

GSH was firstly incubated with 300  $\mu\text{M}$   $\text{K}_2\text{PtCl}_4$  at different molar ratios of  $[\text{GSH}]/[\text{K}_2\text{PtCl}_4]$  in 10 mM

$\text{NaH}_2\text{PO}_4\text{--H}_3\text{PO}_4$  buffer (pH 4.0) for 3 h at 25 °C. Then freshly prepared DMAB aqueous solution was added to the above mixture to reach a final [DMAB]/ $[\text{K}_2\text{PtCl}_4]$  ratio of 5 and followed by a 12-h reduction at 25 °C. Next, an equal volume of aqueous solution of 15.7 mg sonicated GNPs was added to the above mixture. After vibration at 25 °C for 6 h, the resultant was filtered and rinsed by  $\text{NaH}_2\text{PO}_4\text{--H}_3\text{PO}_4$  buffer (pH 4.0) several times and then dried at 60 °C under vacuum for 12 h.

### Synthesis of Pt-Cys/GNPs

#### Method I: adsorption–reduction

Cys was firstly incubated with 300  $\mu\text{M}$   $\text{K}_2\text{PtCl}_4$  at different molar ratios of  $[\text{Cys}]/[\text{K}_2\text{PtCl}_4]$  in 10 mM  $\text{NaH}_2\text{PO}_4\text{--H}_3\text{PO}_4$  buffer (pH 3.0) for 3 h at 25 °C. Then an equal volume of EG containing 15.7 mg sonicated GNPs was added to the above mixture. After vibration for 3 h at 25 °C, the resulting mixture was heated to 125 °C and reacted for 4 h under reflux. Finally, the resultant was filtered and the obtained solid was rinsed several times by  $\text{NaH}_2\text{PO}_4\text{--H}_3\text{PO}_4$  buffer (pH 3.0) and then dried at 60 °C under vacuum for 12 h.

#### Method II: reduction–adsorption

Cys was firstly incubated with 300  $\mu\text{M}$   $\text{K}_2\text{PtCl}_4$  at different molar ratios of  $[\text{Cys}]/[\text{K}_2\text{PtCl}_4]$  in 10 mM  $\text{NaH}_2\text{PO}_4\text{--H}_3\text{PO}_4$  buffer (pH 3.0) for 3 h at 25 °C. Then freshly prepared DMAB aqueous solution was added to the above mixture to reach a final [DMAB]/ $[\text{K}_2\text{PtCl}_4]$  ratio of 5 and followed by a 12-h reduction at 25 °C. Next, an equal volume of aqueous solution of 15.7 mg sonicated GNPs was added to the above mixture. After vibration at 25 °C for 6 h, the resultant was filtered and rinsed by  $\text{NaH}_2\text{PO}_4\text{--H}_3\text{PO}_4$  buffer (pH 3.0) several times and then dried at 60 °C under vacuum for 12 h.

### Electrochemical measurements

Electrochemical measurements of as-prepared Pt-GSH/GNPs and Pt-Cys/GNPs were carried out on an electrochemical workstation (CHI 660E, CH Instruments, China). The workstation was connected to a standard three-electrode cell, with a platinum wire counter electrode and a saturated KCl, Hg/

HgCl<sub>2</sub> reference electrode. A glassy carbon electrode (diameter  $d = 3$  mm, Tianjin Incole Union Technology Co., Ltd) was used as the working electrode. The electrode was firstly polished with  $\text{Al}_2\text{O}_3$  powders with size down to 0.05  $\mu\text{m}$  and then thoroughly rinsed with ultrapure Millipore water and ethanol three times to remove contaminants, respectively. Typically, 1.0 mg of as-prepared catalysts or 0.5 mg commercial Pt/C catalysts was firstly added into the solution comprising of 200  $\mu\text{L}$  of isopropanol, 785  $\mu\text{L}$  of  $\text{H}_2\text{O}$  and 15  $\mu\text{L}$  of Nafion solution (5.0 wt%). Then the obtained mixture was sonicated for 30 min to form a catalyst ink. Next, 5.0  $\mu\text{L}$  of the ink was applied to the surface of a polished glassy carbon and dried on the disk at room temperature for 60 min. Before measuring, the working electrode was activated in a  $\text{N}_2$ -saturated 0.5 M  $\text{H}_2\text{SO}_4$  solution via cyclic voltammetry (CV) between  $-0.2$  and 1.0 V at a scan rate of 50  $\text{mV s}^{-1}$  until it approached a steady state. In the measurement, CV curves of methanol oxidation were recorded in a  $\text{N}_2$ -saturated 0.5 M  $\text{H}_2\text{SO}_4 + 1.0$  M  $\text{CH}_3\text{OH}$  solution at a scan rate of 50  $\text{mV s}^{-1}$  between  $-0.2$  and 1.0 V. Chronoamperometry (CA) tests were carried out at 0.60 V (vs. SCE) for a period of 5000 s. For CO stripping, high-purity CO was bubbled into 0.5 M  $\text{H}_2\text{SO}_4$  for 30 min with the electrode potential of 0 V versus SCE. Then dissolved CO was purged out of the electrolyte by bubbling  $\text{N}_2$  for another 30 min. CVs were recorded for all the catalysts between  $-0.2$  and 1.0 V at 50  $\text{mV s}^{-1}$ . All experiments were done at room temperature.

The electrochemical surface areas (ECSA) of as-prepared catalysts were evaluated by measuring coulombic charges collected in the hydrogen adsorption and desorption region between  $-0.2$  and 0.1 V. The ECSA values were calculated according to  $\text{ECSA} = Q_{\text{H}} / (0.21 \times m_{\text{Pt}})$ , where  $m_{\text{Pt}}$  is the Pt loading ( $\text{mg cm}^{-2}$ ) on the working electrode;  $Q_{\text{H}}$  ( $\text{mC cm}^{-2}$ ) was obtained by integrating the corrected hydrogen adsorption/desorption region and then divided by the used scan rate; 0.21  $\text{mC cm}^{-2}$  is required charge to oxidize a monolayer of hydrogen on a smooth Pt surface [24]. In the CV curves of methanol oxidation, the peak current density in the forward scan ( $I_f$ ) and in the reverse scan ( $I_b$ ) was attributed to the dehydrogenation of methanol and the removal of some intermediate carbonaceous species (poisoning species), respectively [25]. The ratios of  $I_f/I_b$  were used

to evaluate the contamination arising from poisoning species.

### Characterizations

The dispersity and distribution of as-prepared catalysts were analyzed by using transmission electron microscopy (TEM) and high-resolution TEM (HRTEM), which were conducted on a Tecnai JEM-

2100F TEM (JEOL; Japan) with an accelerating voltage of 200 kV. All the samples were prepared by depositing a drop of suspended catalysts diluted in ethanol onto a copper grid coated with carbon film. Electron energy loss spectroscopy (EELS) was performed to identify the elemental distribution of as-prepared catalysts.

Isothermal titration calorimetry (ITC) experiments were performed using a MicroCal VP-ITC (MicroCal,

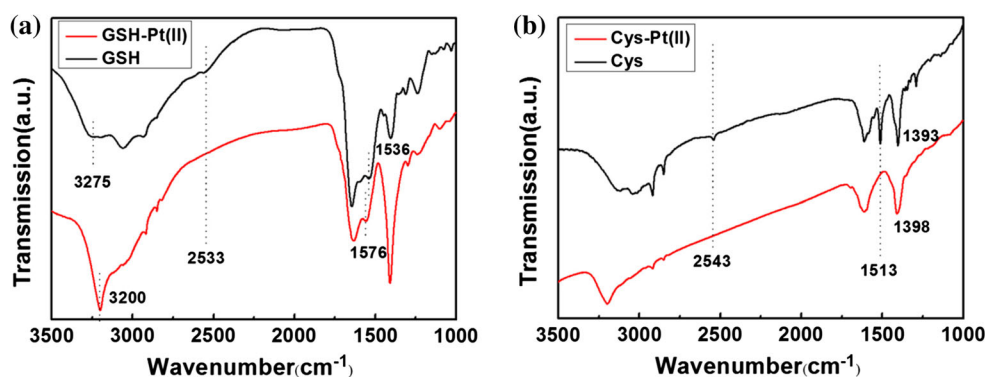


**Figure 1** FT-IR spectra of **a** GSH and GSH-Pt(II) ( $[K_2PtCl_4]/[GSH] = 12$ , pH 4.0), **b** Cys and Cys-Pt(II) ( $[K_2PtCl_4]/[Cys] = 24$ , pH 3.0).

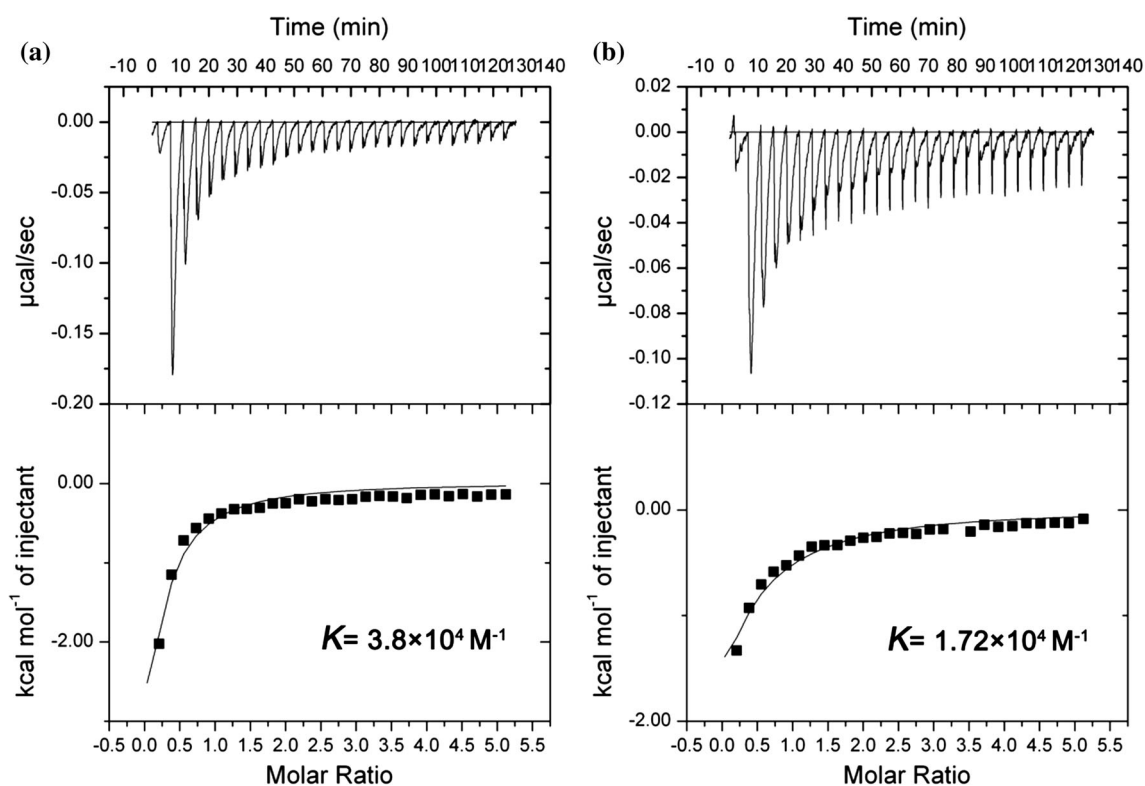
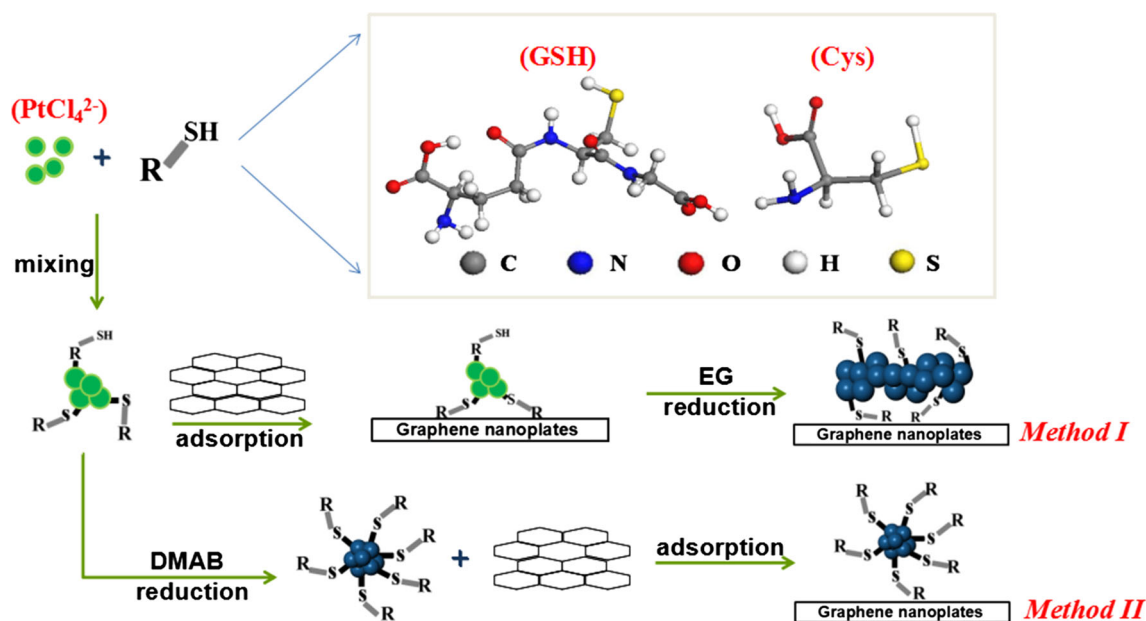


**Figure 2** ITC analysis of 40  $\mu$ M. **a** GSH (pH 4.0) and **b** Cys (pH 3.0) titrated with  $K_2PtCl_4$  solution (1 mM) at 25  $^{\circ}$ C.



**Scheme 1** Schematic illustration of two synthesis methods proposed in this study.

Northampton, MA) with the sample cell (1.45 mL) containing 40  $\mu\text{M}$  GSH in 10 mM  $\text{NaH}_2\text{PO}_4\text{-H}_3\text{PO}_4$  buffer (pH 4.0) or 40  $\mu\text{M}$  Cys in 10 mM  $\text{NaH}_2\text{PO}_4\text{-H}_3\text{PO}_4$  buffer (pH 3.0). Typically, 27 serial injections of 1 mM  $\text{K}_2\text{PtCl}_4$  dissolved in  $\text{NaH}_2\text{PO}_4\text{-H}_3\text{PO}_4$  buffer (pH 4.0 for GSH and pH 3.0 for Cys) of 10  $\mu\text{L}$  volume each were titrated in the sample cell at an interval of 270 s under continuous stirring at 307 rpm.

FT-IR spectra were recorded on a Thermo Scientific Nicolet iS10 FT-IR spectrometer. The samples were dropped onto the ZnSe transparent supports and dried in the drying oven.

X-ray photoelectron spectroscopy (XPS) was performed on a PHI5000 Versaprobe. In the sample preparation, 30  $\mu\text{L}$  of sample solution (0.2 mg/mL) was added dropwise onto a clean silicon wafer, which was subsequently dried under a nitrogen gas atmosphere. This operation was repeated thrice to obtain the specimens.

Zeta potentials ( $\zeta$ ) of GNPs were measured at different pH in the mixture of water and EG (1:1) at the concentration of 0.05 mg/mL by dynamic light scattering (DLS, Malvern Nano-ZS, UK).

The amounts of metal loading in different catalysts were measured by inductively coupled plasma optical emission spectrometry (ICP-OES, Thermo Jarrell-Ash Corp, USA).

## Results and discussion

### Molecular interactions of biothiols with Pt(II) precursors

Molecular interactions between biothiols and  $\text{K}_2\text{PtCl}_4$  were investigated by FT-IR and ITC analysis. According to the FT-IR spectra shown in Fig. 1a, typical S-H stretching at  $2533\text{ cm}^{-1}$  disappears after incubation with  $\text{K}_2\text{PtCl}_4$ . In the meanwhile, the red shift from  $1536$  to  $1576\text{ cm}^{-1}$  as well as the blue shift from  $3275$  to  $3200\text{ cm}^{-1}$  suggests that Pt(II) also interacts with  $-\text{COOH}$  and  $-\text{NH}_2$  groups [26]. As shown in Fig. 1b, both the N-H bending vibration at  $1513\text{ cm}^{-1}$  and the S-H stretching at  $2543\text{ cm}^{-1}$  disappear upon addition of the precursor. Additionally, a red shift from  $1393$  to  $1398\text{ cm}^{-1}$  was also detected, demonstrating the coordination of Pt(II) with  $-\text{SH}$ ,  $-\text{NH}_2$  as well as  $-\text{COOH}$  groups of Cys [27]. Through ITC analysis (Fig. 2), the binding constants ( $K$ ) were calculated as  $3.8 \times 10^4$  and  $1.72 \times 10^4\text{ M}^{-1}$  for GSH and Cys, respectively.

### Characterizations and electrochemical performance of Pt-GSH/GNPs

Two synthesis methods were employed to prepare Pt-GSH/GNPs catalysts, namely “adsorption–reduction (method I)” and “reduction–adsorption (method II),”

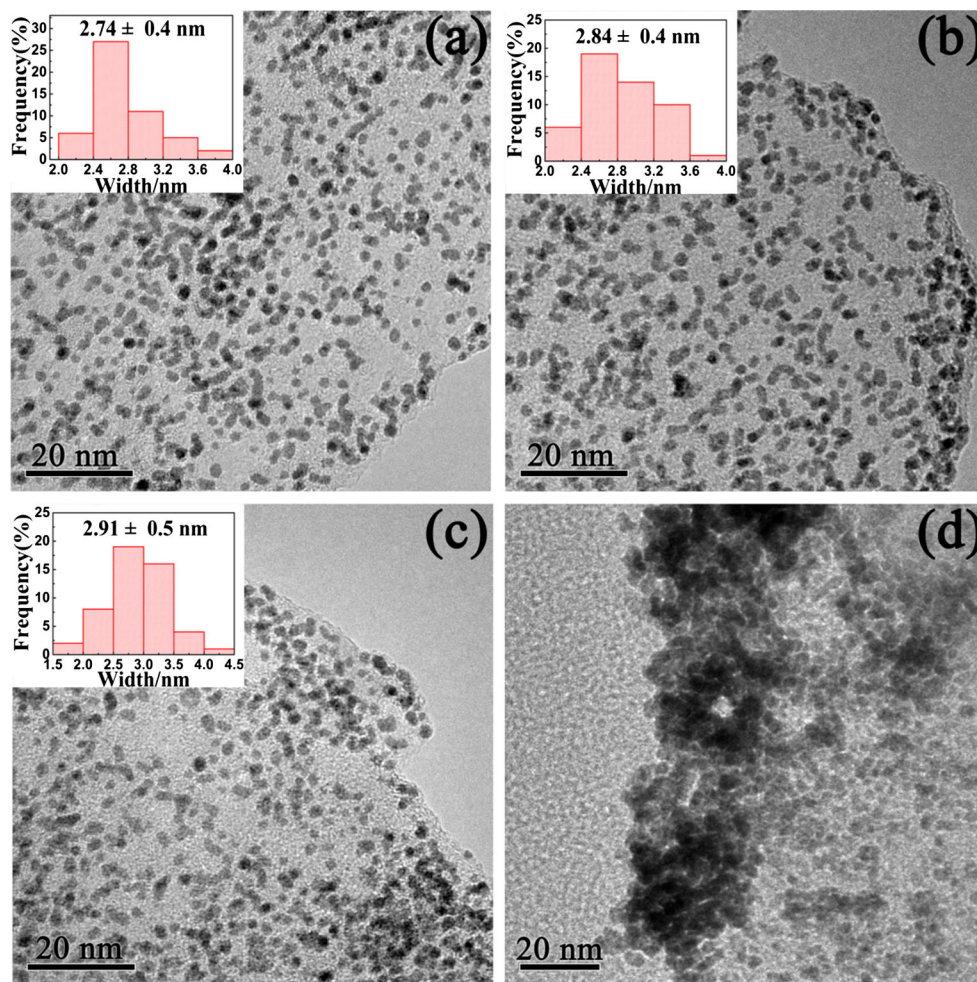


**Figure 3** TEM images of Pt-GSH/GNPs prepared by *method I* at different ratios of  $[K_2PtCl_4]/[GSH]$ : **a** 3, **b** 12, **c** 24, **d** Pt/GNPs.

**Table 1** Loading of Pt determined by ICP-OES and the mean particle size determined by TEM

Catalysts	Pt (wt%)	Diameter/width (nm)
Pt/C-JM <sup>a</sup>	19.42	3.09
Pt/GNPs <sup>b</sup>	7.51	4.1
Pt-GSH(3:1)/GNPs ( <i>method I</i> )	8.92	2.74
Pt-GSH(12:1)/GNPs ( <i>method I</i> )	8.71	2.84
Pt-GSH(24:1)/GNPs ( <i>method I</i> )	8.3	2.91
Pt-GSH(3:1)/GNPs ( <i>method II</i> )	5.15	2.63
Pt-GSH(12:1)/GNPs ( <i>method II</i> )	5.51	3.04
Pt-GSH(24:1)/GNPs ( <i>method II</i> )	5.93	3.2

<sup>a</sup> Commercial Pt/C

<sup>b</sup> Catalyst prepared by *method I* without using GSH or Cys

respectively (illustrated in Scheme 1). In *method I*, GSH-Pt(II) complexes were firstly adsorbed onto the GNPs at pH 4.0 through electrostatic interactions as opposite charge of two substances (Fig. S1). Then the growth of Pt NPs was oriented by both GSH and

GNPs. For comparison, in *method II*, monodisperse Pt NPs were firstly synthesized in aqueous solution under the protection of GSH. Then as-prepared Pt NPs were adsorbed onto the GNPs to obtain Pt-GSH/GNPs.

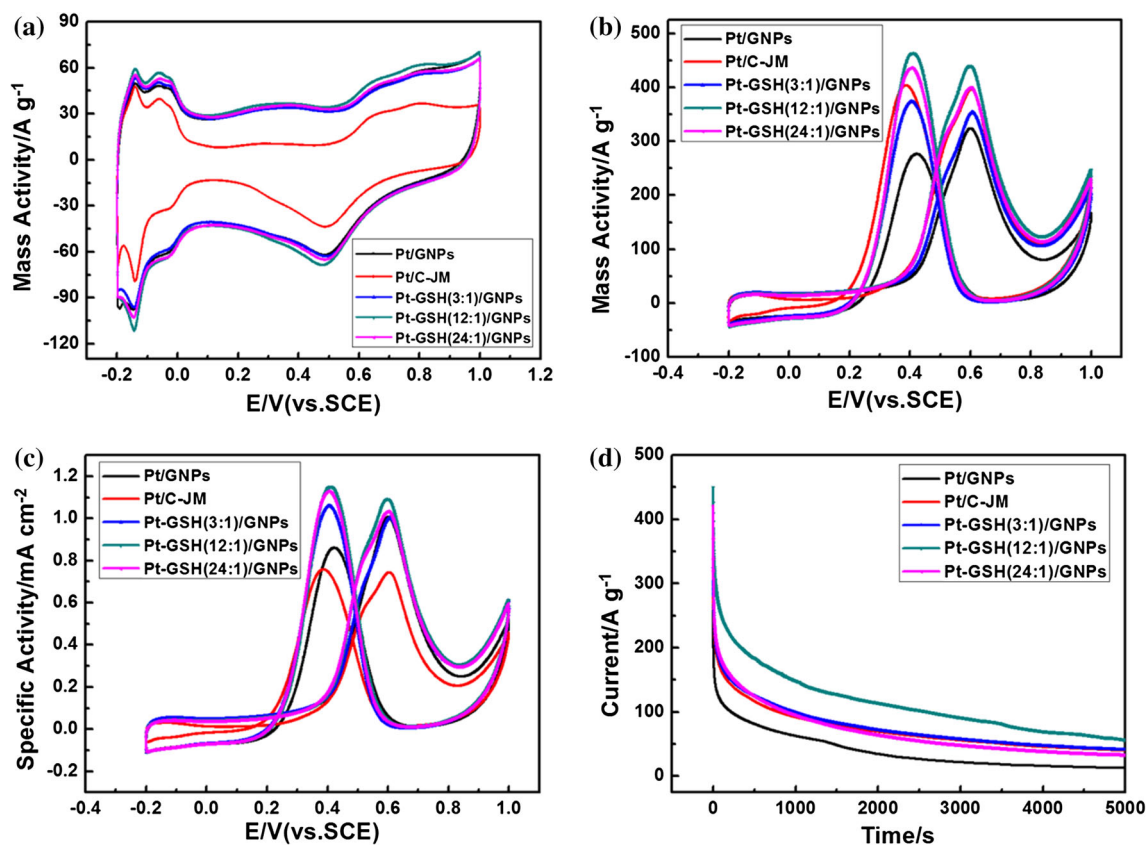


**Figure 4** a CV curves of Pt-GSH/GNPs prepared by *method I* in 0.5 M H<sub>2</sub>SO<sub>4</sub> at 50 mV s<sup>-1</sup>, b mass activities, c specific activities of MOR recorded in 0.5 M H<sub>2</sub>SO<sub>4</sub> + 1.0 M CH<sub>3</sub>OH at 50 mV s<sup>-1</sup>, d chronoamperometric curves of different catalysts tested at 0.6 V.

**Table 2** ECSA and  $I_f/I_b$  of Pt-GSH/GNPs prepared by *method I* and *method II*

Catalysts	ECSA/m <sup>2</sup> g <sup>-1</sup>	$I_f/I_b$
Pt/C-JM	53.3	0.97
Pt/GNPs	32.12	1.16
Pt-GSH(3:1)/GNPs ( <i>method I</i> )	35.26	0.94
Pt-GSH(12:1)/GNPs ( <i>method I</i> )	40.27	0.96
Pt-GSH(24:1)/GNPs ( <i>method I</i> )	38.65	0.92
Pt-GSH(3:1)/GNPs ( <i>method II</i> )	32.52	1.15
Pt-GSH(12:1)/GNPs ( <i>method II</i> )	38.17	1.07
Pt-GSH(24:1)/GNPs ( <i>method II</i> )	34.15	1.03

In *method I*, by employing EG as a mild reductant, Pt-GSH/GNPs were prepared through the hydrothermal synthesis at different molar ratios of [K<sub>2</sub>PtCl<sub>4</sub>]/[GSH]. According to TEM images (Fig. 3 and Fig. S2), non-spherical Pt NPs uniformly disperse on the surface of GNPs. At the [K<sub>2</sub>PtCl<sub>4</sub>]/[GSH] ratio of 24, 12 and 3, the obtained Pt-GSH/GNPs show the average width of 2.91, 2.84 and 2.74 nm, respectively, with the length ranging in 3–8 nm (Table 1). In

contrast, a significant aggregation was observed for Pt/GNPs without the orientation of GSH, indicating the critical role of –SH, –COOH and –NH<sub>2</sub> groups in the synthesis of dispersive Pt NPs on GNPs. For comparative study, the Pt-GSH/GNPs obtained through *method II* exhibit spherical morphologies, with the average diameter ranging from 2.6 to 3.2 nm (Table 1 and Fig. S3).

All the catalysts exhibit typical electrochemical behaviors of Pt in a 0.5 M nitrogen-saturated H<sub>2</sub>SO<sub>4</sub> solution, as shown in Fig. 4a and Table 2. Pt-GSH/GNPs obtained from two methods show higher ECSA than that of Pt/GNPs, suggesting more catalytically active sites available for electrochemical reaction. The Pt-GSH/GNPs prepared through *method I* have comparable  $I_f/I_b$  values with Pt/C-JM, whereas the Pt-GSH/GNPs obtained by *method II* possess a little higher  $I_f/I_b$  than Pt/C-JM.

According to the  $I_f$  values shown in Fig. 4b, Pt-GSH(12:1)/GNPs exhibited the highest mass activity, which is 1.1 times higher than that of Pt/C-JM (396 A g<sup>-1</sup>) and 1.4 times than Pt/GNPs (323 A g<sup>-1</sup>).

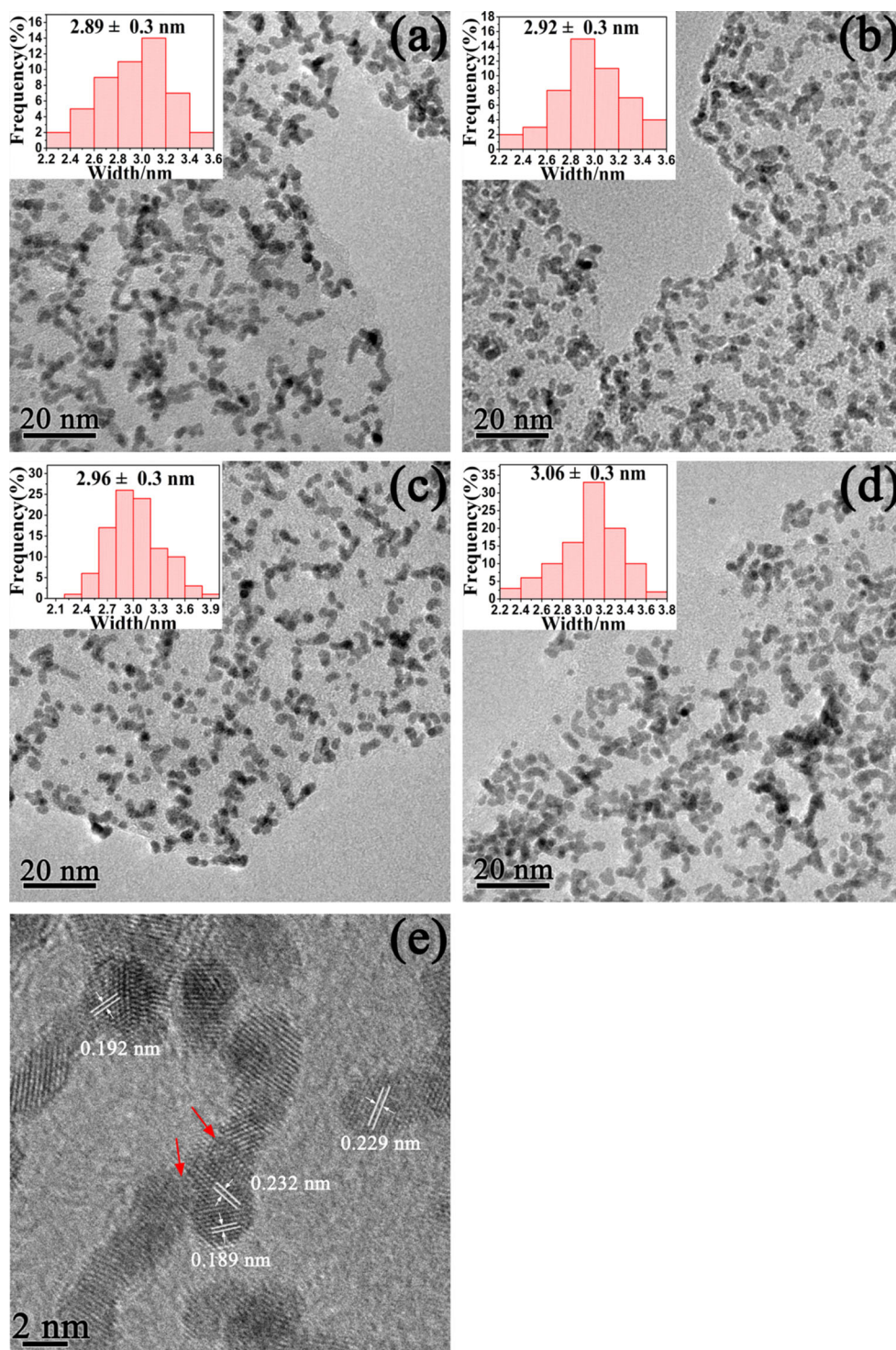


**Figure 5** TEM images of Pt-Cys/GNPs prepared by *method I* at different ratios of  $[K_2PtCl_4]/[Cys]$ : **a** 6, **b** 12, **c** 24, **d** 48, **e** HRTEM image of Pt-Cys/GNPs at  $[K_2PtCl_4]/[Cys] = 24$ .

Besides, the specific activity of Pt-GSH(12:1)/GNPs is  $1.09 \text{ mA cm}^{-2}$ , which is 1.5 and 1.1 times higher than those of Pt/C-JM ( $0.74 \text{ mA cm}^{-2}$ ) and Pt/GNPs ( $1.0 \text{ mA cm}^{-2}$ ), respectively (Fig. 4c). The stabilities

of Pt-GSH/GNPs were estimated by chronoamperometric measurements at a potential of 0.6 V for 5000 s. As shown in Fig. 4d, Pt-GSH(12:1)/GNPs exhibit a slower current decay and a higher current



**Table 3** Loading of Pt determined by ICP-OES and the mean particle size determined by TEM

Catalysts	Pt (wt%)	Width (nm)
Pt-Cys(6:1)/GNPs	8.77	2.89
Pt-Cys(12:1)/GNPs	8.53	2.92
Pt-Cys(24:1)/GNPs	8.46	2.96
Pt-Cys(48:1)/GNPs	8.36	3.06

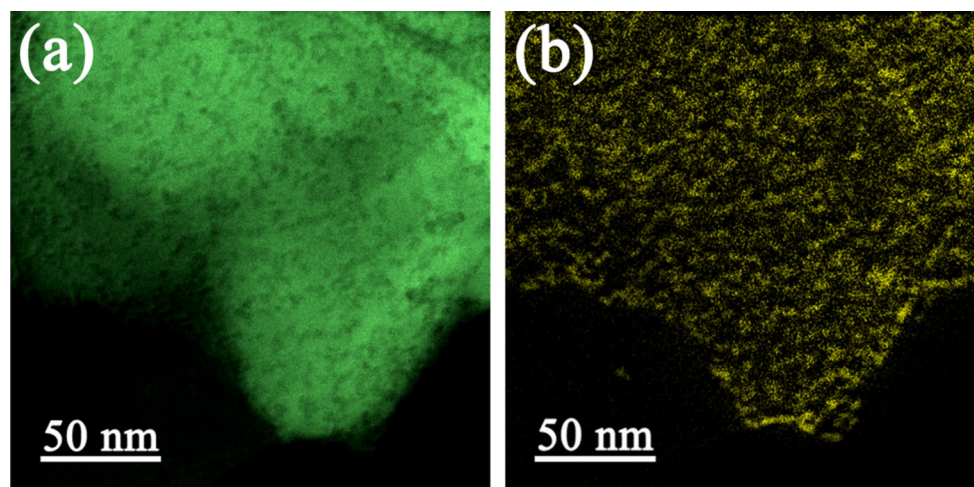
density in MOR as compared to other catalysts, suggesting longer operation time and higher antipoisoning ability. Moreover, CO stripping measurements were applied to reveal their antipoisoning abilities. Obviously, all the biothiol-containing catalysts exhibit lower peak potentials as compared to Pt/GNPs and Pt/C-JM (Fig. S4), which demonstrates that addition of biothiols improves the antipoisoning properties of Pt catalysts. Compared with the catalytic performance of sphere-like Pt NPs synthesized in aqueous solution through *method II* (Fig. S5), it is reasonable to conclude that non-spherical Pt NPs can facilitate the electron transfer during electrochemical reactions [28–30].

### Characterizations and electrochemical performance of Pt-Cys/GNPs

Two synthesis methods described above were also used to prepare Pt-Cys/GNPs. As shown in Fig. 5 and Table 3, non-spherical Pt NPs uniformly disperse on the surface of GNPs at different ratios of  $[K_2PtCl_4]/[Cys]$ , with the average width of approximate 3 nm and the length of 3–13 nm. HRTEM image

reveals that the non-spherical NPs in the Pt-Cys(24:1)/GNPs are actually composed of multiple single-crystalline segments (Fig. 5e). The lattice distances of 0.23 and 0.19 nm correspond well to the (111) and (100) lattice spacing of face-centered cubic Pt, respectively. In addition, grain boundaries can be evidently observed between adjacent particles, as marked by red arrows. It has been reported that the presence of grain boundaries could serve as possible catalytic sites and transport channels for reactants and therefore effectively improve the electrocatalytic activities [31]. Meanwhile, the distribution of Cys on the as-prepared catalysts was evaluated by EELS mapping (Fig. 6). The element S from Cys is uniformly distributed on the GNPs, which further confirms the Cys-oriented growth of Pt NPs. As a control, Pt NPs synthesized in the aqueous solution through *method II* (Fig. S6) display a serious agglomeration, suggesting that in the absence of GNPs the individual Cys cannot function well to modulate the dispersity of Pt NPs and there exists a synergistic effect between GNPs and Cys in the growth of Pt NPs.

To understand deeply the surface properties of as-prepared Pt-Cys/GNPs by *method I*, the charge states of Pt species were analyzed by XPS spectra, as listed in Table 4. In the analyzing spectra (Fig. S7), it is assumed that the doublets have Gaussian-shaped (5/2–7/2) components of equal half-widths with an intensity ratio of ca. 3:4, and the Pt(4f) spin splitting energy was about 3.3 eV. The binding energy of the electron on the Pt 4f<sub>7/2</sub> orbitals can be deconstructed into Pt<sup>2+</sup> and Pt<sup>0</sup> components. As the ratio of

**Figure 6** Element mapping of a C and b S of Pt-Cys(24:1)/GNPs by EELS.

**Table 4** Binding energies and relative content of Pt species in Pt-Cys/GNPs by *method I* determined by XPS spectra

Catalysts	Pt <sup>0</sup> (eV) %		Pt <sup>2+</sup> (eV) %	
	4f7/2	4f5/2	4f7/2	4f5/2
Pt-Cys(6:1)/GNPs	71.5 (46.69)	74.9	72.7 (53.31)	75.9
Pt-Cys(12:1)/GNPs	71.4 (48.67)	74.7	72.7 (51.33)	75.9
Pt-Cys(24:1)/GNPs	71.5 (54.72)	74.9	72.8 (45.28)	76.1
Pt-Cys(48:1)/GNPs	71.6 (56.83)	74.9	72.9 (43.17)	76.1

**Table 5** ECSA and  $I_f/I_b$  of Pt-Cys/GNPs prepared by *method I*

Catalysts	ECSA/m <sup>2</sup> g <sup>-1</sup>	$I_f/I_b$
Pt-Cys(6:1)/GNPs	39.62	1.02
Pt-Cys(12:1)/GNPs	41.95	1.06
Pt-Cys(24:1)/GNPs	45.62	1.09
Pt-Cys(48:1)/GNPs	42.36	0.97

[K<sub>2</sub>PtCl<sub>4</sub>]/[Cys] increases from 6 to 48, the fractions of Pt<sup>0</sup> species increase from 46.7 to 56.8%.

The electrochemical performance of Pt-Cys/GNPs synthesized by *method I* is listed in Table 5 and Fig. 7a. The Pt-Cys(24:1)/GNPs show the highest ECSA value of 45.62 m<sup>2</sup> g<sup>-1</sup>, which is 1.4 fold than that of Pt/GNPs. In the CV curves of methanol oxidation (Fig. 7b), the Pt-Cys(24:1)/GNPs exhibit 1.8- and 2.2-fold higher mass activities as compared to the Pt/C-JM and the Pt/GNPs, respectively. As shown in Fig. 7c, the peak current density of Pt-Cys(24:1)/GNPs (1.52 mA cm<sup>-2</sup>) is 2.1 and 1.5 times than that of Pt/C-JM and Pt/GNPs, respectively. Among all the as-prepared catalysts (Fig. 7d), the Pt-Cys(24:1)/GNPs possess the highest stability as well as anti-poisoning ability in MOR.

### Comparisons of Pt/GNPs toward morphologies and activities

Regarding both physicochemical properties and electrochemical performance of Pt-GSH/GNPs based

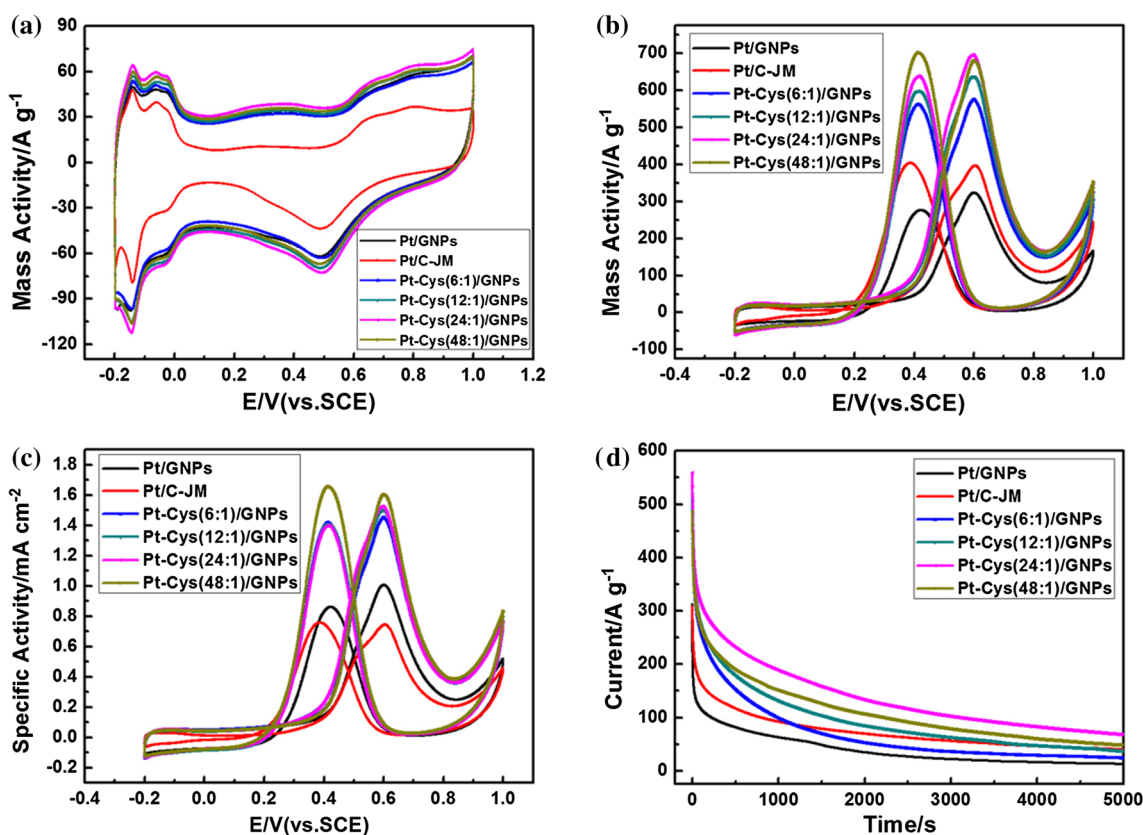


**Figure 7** a CV curves of Pt-Cys/GNPs prepared by *method I* in 0.5 M H<sub>2</sub>SO<sub>4</sub> at 50 mV s<sup>-1</sup>, b mass activities, c specific activities of MOR recorded in 0.5 M H<sub>2</sub>SO<sub>4</sub> + 1.0 M CH<sub>3</sub>OH at 50 mV s<sup>-1</sup>, d chronoamperometric curves of different catalysts tested at 0.6 V.

on two different methods, we can conclude that the complexes of biothiol/GNPs through electrostatic adsorption can act as an effective template that facilitates the growth of non-spherical Pt NPs. In comparison, monodisperse Pt spheres were liable to form in aqueous solution without the guidance of hybrid templates, which reveals a cooperative effect between carbon supports and biothiols on the morphologies of Pt nanostructures.

The advantages of non-spherical Pt NPs in MOR were exemplified by Pt-Cys/GNPs with the average width of 3 nm and the length ranging in 3–13 nm, which possess higher catalytic activity than Pt-GSH/GNPs (2.9 nm in width, 3–8 nm in length). Previous reports have shown that 1D Pt NPs have advantages in electrochemical reactions over zero-dimensional nanocatalysts [32]. For example, Li and coworkers used polyethylene glycol monooleyl ether (Brij-35) as a growth-directing agent for the fabrication of reduced graphene oxide-supported worm-like Au-Pd nanostructures with an average width of 2 nm and length of 10 nm, which showed improved analytical performance for nitrite detection [33]. Therefore, it is reasonable to conclude that the catalytic activities of GNP-supported Pt NPs are greatly associated with surface functional groups, particle sizes as well as morphologies.

## Conclusions

Highly dispersive Pt nanoparticles on GNPs were controllably synthesized under the orientation of different biothiols. It is demonstrated that the electrochemical performance of GNPs-supported Pt NPs is greatly associated with thiol-containing groups, particle sizes as well as morphologies. Biothiols and GNPs cooperatively act as effective templates to assist Pt(II)-precursor depositing uniformly on the surface of GNPs, contributing to non-spherical nanostructures. In contrast, spherical Pt NPs were obtained through aqueous synthesis, which exhibit lower activities as compared to non-spherical Pt NPs. Adopting Cys as active sites, Pt NPs with the average width of 3 nm and the length ranging in 3–13 nm display the highest catalytic activities in methanol electrooxidation, which possess 1.8-fold mass activity, better stability and lower CO poisoning susceptibility than that of commercial Pt/C.

## Acknowledgement

This work was supported by the NSFC (21576205, 21621004) and the Program for Changjiang Scholars and Innovative Research Team in University (IRT\_15R46).

## Compliance with ethical standards

**Conflict of interest** The authors declare that they have no conflict of interest.

**Electronic supplementary material:** The online version of this article (doi:10.1007/s10853-017-1508-5) contains supplementary material, which is available to authorized users.

## References

- [1.] Li G, Jiang L, Zhang B, Jiang Q, Su DS, Sun G (2013) A highly active porous Pt–PbOx/C catalyst toward alcohol electro-oxidation in alkaline electrolyte. *Int J Hydrog Energy* 38:12767–12773
- [2.] Ghavidel MRZ, Easton EB (2015) Thermally induced changes in the structure and ethanol oxidation activity of Pt<sub>0.25</sub>Mn<sub>0.75</sub>/C. *Appl Catal B* 176:150–159
- [3.] Qi Z, Xiao C, Liu C, Goh TW, Zhou L, Ganesh RM, Pei Y, Li X, Curtiss LA, Huang W (2017) Sub-4 nm PtZn intermetallic nanoparticles for enhanced mass and specific activities in catalytic electrooxidation reaction. *J Am Chem Soc* 139:4762–4768
- [4.] Nie Y, Li L, Wei Z (2015) Recent advancements in Pt and Pt-free catalysts for oxygen reduction reaction. *Chem Soc Rev* 44:2168–2201
- [5.] Hsu CH, Liao HY, Wu YF, Kuo PL (2011) Benzylamine-assisted noncovalent exfoliation of graphite-protecting Pt nanoparticles applied as catalyst for methanol oxidation. *ACS Appl Mater Interfaces* 3:2169–2172
- [6.] Zhang G, Yang Z, Huang C, Zhang W, Wang Y (2015) Small-sized and highly dispersed Pt nanoparticles loading on graphite nanoplatelets as an effective catalyst for methanol oxidation. *Nanoscale* 7:10170–10177
- [7.] Li S, Ma J, Huo H, Jin J, Ma J, Yang H (2016) Ionic liquids-noncovalently functionalized multi-walled carbon nanotubes decorated with palladium nanoparticles: a promising electrocatalyst for ethanol electrooxidation. *Int J Hydrog Energy* 41:12358–12368
- [8.] Luo F, Ling Y, Zhang Q, Yu X, Liu Q, Yang Z (2017) Carbon paper-free membrane electrode assembly fabricated

- from a Pt electrocatalyst supported on multi-walled carbon nanotubes. *J Mater Sci* 52:8412–8420. doi:10.1007/s10853-017-1081-y
- [9.] Ran X, Yang L, Qu Q, Li S, Chen Y, Zuo L, Li L (2017) Synthesis of well-dispersive 2.0 nm Pd–Pt bimetallic nanoclusters supported on  $\beta$ -cyclodextrin functionalized graphene with excellent electrocatalytic activity. *RSC Adv* 7:1947–1955
- [10.] Chen M, Meng Y, Zhou J, Diao G (2014) Platinum nanoworms self-assemble on  $\beta$ -cyclodextrin polymer inclusion complexes functionalized reduced graphene oxide as enhanced catalyst for direct methanol fuel cells. *J Power Sources* 265:110–117
- [11.] Zhang G, Huang C, Qin R, Shao Z, An D, Zhang W, Wang Y (2015) Uniform Pd–Pt alloy nanoparticles supported on graphite nanoplatelets with high electrocatalytic activity towards methanol oxidation. *J Mater Chem A* 3:5204–5211
- [12.] Guo CX, Zhang LY, Miao J, Zhang J, Li CM (2013) DNA-functionalized graphene to guide growth of highly active Pd nanocrystals as efficient electrocatalyst for direct formic acid fuel cells. *Adv Energy Mater* 3:167–171
- [13.] Li M, Pan Y, Guo X, Liang Y, Wu Y, Wen Y, Yang H (2015) Pt/single-stranded DNA/graphene nanocomposite with improved catalytic activity and CO tolerance. *J Mater Chem A* 3:10353–10359
- [14.] Li X, Wei J, Chai Y, Zhang S, Zhou M (2015) Different polyaniline/carbon nanotube composites as Pt catalyst supports for methanol electro-oxidation. *J Mater Sci* 50:1159–1168. doi:10.1007/s10853-014-8672-7
- [15.] Farrag M (2016) Preparation, characterization and photocatalytic activity of size selected platinum nanoclusters. *J Photochem Photobiol A* 318:42–50
- [16.] Chang Y, Zhang Z, Hao J, Yang W, Tang J (2016) BSA-stabilized Au clusters as peroxidase mimetic for colorimetric detection of Ag<sup>+</sup>. *Sens Actuators B* 232:692–697
- [17.] Kumar N, Upadhyay LSB (2016) Facile and green synthesis of highly stable L-cysteine functionalized copper nanoparticles. *Appl Surf Sci* 385:225–233
- [18.] Eklund SE, Cliffel DE (2004) Synthesis and catalytic properties of soluble platinum nanoparticles protected by a thiol monolayer. *Langmuir* 20:6012–6018
- [19.] Sharma S, Kim B, Lee D (2012) Water-soluble Pd nanoparticles capped with glutathione: synthesis, characterization, and magnetic properties. *Langmuir* 28:15958–15965
- [20.] Kwak K, Choi W, Tang Q, Kim M, Lee Y, Jiang DE, Lee D (2017) A molecule-like PtAu<sub>24</sub>(SC<sub>6</sub>H<sub>13</sub>)<sub>18</sub> nanocluster as an electrocatalyst for hydrogen production. *Nat Commun* 8:14723–14730
- [21.] Chen Y, Zeng C, Kauffman DR, Jin R (2015) Tuning the magic size of atomically precise gold nanoclusters via isomeric methylbenzenethiols. *Nano Lett* 15:3603–3609
- [22.] Fu Y, Zhang H, Dai S, Zhi X, Zhang J, Li W (2015) Glutathione-stabilized palladium nanozyme for colorimetric assay of silver(I) ions. *Analyst* 140:6676–6683
- [23.] Zhou M, Zeng C, Chen Y, Zhao S, Sfeir MY, Zhu M, Jin R (2016) Evolution from the plasmon to exciton state in ligand-protected atomically precise gold nanoparticles. *Nat Commun* 7:13240–13246
- [24.] Lim B, Jiang M, Camargo PHC, Cho EC, Tao J, Lu X, Zhu Y, Xia Y (2009) Pd–Pt bimetallic nanodendrites with high activity for oxygen reduction. *Science* 324:1302–1305
- [25.] Chen Q, Zhang J, Jia Y, Jiang Z, Xie Z, Zheng L (2014) Wet chemical synthesis of intermetallic Pt<sub>3</sub>Zn nanocrystals via weak reduction reaction together with UPD process and their excellent electrocatalytic performances. *Nanoscale* 6:7019–7024
- [26.] Zhang L, Xu C, Li B (2009) Simple and sensitive detection method for chromium(VI) in water using glutathione-capped CdTe quantum dots as fluorescent probes. *Microchim Acta* 166:61–68
- [27.] Soomro RA, Nafady A, Sirajuddin Memon N, Sherazi TH, Kalwar NH (2014) L-cysteine protected copper nanoparticles as colorimetric sensor for mercuric ions. *Talanta* 130:415–422
- [28.] Liao Y, Yu G, Zhang Y, Guo T, Chang F, Zhong CJ (2016) Composition-tunable PtCu alloy nanowires and electrocatalytic synergy for methanol oxidation reaction. *J Phys Chem C* 120:10476–10484
- [29.] Xu J, Wang ZH, Li HH, Liu JW, Yu SH (2016) Templating synthesis of ternary PtPdTe nanowires with tunable diameter for methanol electrooxidation. *CrystEngComm* 18:4038–4041
- [30.] Hong W, Wang J, Wang E (2014) Dendritic Au/Pt and Au/PtCu nanowires with enhanced electrocatalytic activity for methanol electrooxidation. *Small* 10:3262–3265
- [31.] Wang S, Jiang SP, Wang X, Guo J (2011) Enhanced electrochemical activity of Pt nanowire network electrocatalysts for methanol oxidation reaction of fuel cells. *Electrochim Acta* 56:1563–1569
- [32.] Xia BY, Wu HB, Yan Y, Lou XW, Wang X (2013) Ultrathin and ultralong single-crystal platinum nanowire assemblies with highly stable electrocatalytic activity. *J Am Chem Soc* 135:9480–9485
- [33.] Li SS, Hu YY, Wang AJ, Weng X, Chen JR, Feng JJ (2015) Simple synthesis of worm-like Au–Pd nanostructures supported on reduced graphene oxide for highly sensitive detection of nitrite. *Sens Actuators B* 208:468–474